

Short Communication

Solvo-Thermal Synthesis of $H_6V_4O_{10}$ Microspheres as Stable Electrode Materials for Lithium and Zinc-ion Batteries

Hailong Fei^{1,2}

¹ Colloge of Chemistry, Fuzhou University, Fuzhou, Fujian 350002, China.

²Key Laboratory of Advanced Energy Materials Chemistry (Ministry of Education), Nankai University, Tianjin 300071.

E-mail: fimer99@163.com

Received: 5 July 2019 / Accepted: 12 September 2019 / Published: 29 October 2019

$NH_4V_4O_{10}$ based ammonium vanadium bronze has been widely investigated as a cathode material for lithium-ion batteries. A V_4O_{10} group based $H_6V_4O_{10}$ might be a potential anode material due to its high hydrogen content and similar composition. Microspheres modified by loosely distributed nanoparticles showed higher discharge capacity and better cycling stability than those composed of tightly packed micro-blocks for lithium-ion batteries and zinc-ion batteries. The former can steadily cycle at current densities of 400 mA g^{-1} for 1000 cycles with a capacity of up to 387 mA h g^{-1} . The discharge capacity of aqueous zinc-ion batteries can be up to $238.8 \text{ mA h g}^{-1}$ with a capacity retention of 87.8% after 26 cycles. The improved electrochemical performance can be ascribed to the nanoparticles modifying the loose surface, which promotes ion and electron transfer.

Keywords: Hydrogen Vanadate; Microspheres; Anode

1. INTRODUCTION

Currently, great interest has been drawn to lithium-ion and aqueous zinc-ion batteries for their huge advantages towards the application of large-scale energy storage, abundance, cost effectiveness and safety [1]. Vanadium oxides [2, 3], vanadate [4] and ammonium vanadium bronzes [5-8] have been widely investigated as electrode materials for lithium, sodium and magnesium-ion batteries because of their high capacity, easy synthesis and versatile crystal structures. $NH_4V_4O_{10}$ -based ammonium vanadium bronze has been well known as an electrode material for lithium and zinc-ion batteries. High concentrations of hydrogen atoms in $\alpha\text{-}V_2O_5$ can improve the kinetics of ionic and electronic transport, electronic conductivity and smaller volume expansion [9]. Therefore, $H_6V_4O_{10}$ might be a potential electrode material for lithium and zinc-ion batteries with a high-content of hydrogen. It is reported that

$\text{H}_6\text{V}_4\text{O}_{10}$ can be prepared via adsorbing H_2 on V_2O_5 at high temperature. For example, platinum-activated V_2O_5 reacts with hydrogen at approximately $150\text{ }^\circ\text{C}$ to give $\text{H}_3\text{V}_2\text{O}_5$. The hydrogen insertion creates distortion in the orthorhombic structure of V_2O_5 and decreases the crystal symmetry by forming a monoclinic phase with a composition of $\text{H}_6\text{V}_4\text{O}_{10}$ at $426\text{ }^\circ\text{C}$ [10]. However, the synthesis and application of $\text{H}_6\text{V}_4\text{O}_{10}$ has seldom been reported since 1988. Recently, sphere-like metal oxides and hollow structures have shown high specific capacity, excellent rate capability, and outstanding cycling performance due to their unique structural features and rich chemical properties [11,12]. Herein, we develop a facile solvo-thermal method to prepare $\text{H}_6\text{V}_4\text{O}_{10}$ microspheres. A mixed solvent of ethylene glycol and polyethylene glycol 400 promotes the formation of a vanadyl glycolate precursor, which can be converted to rare $\text{H}_6\text{V}_4\text{O}_{10}$ instead of V_2O_5 microspheres under certain conditions. Furthermore, it is a facile method to prepare $\text{H}_6\text{V}_4\text{O}_{10}$ microspheres with different surface morphologies on a large scale. Herein, plate-assembled irregular $\text{H}_6\text{V}_4\text{O}_{10}$ microflowers are prepared under hydrothermal conditions via a reduction of V_2O_5 by ascorbic acid [13]. When tested as an electrode material for lithium-ion batteries and aqueous zinc-ion batteries, it showed high discharge capacity and good cycling stability.

2. EXPERIMENTAL

Masses of 0.59 g ammonium vanadate and 0.16 g oxalic acid were added to a mixed solvent of polyethylene glycol 400 (PEG 400, $\text{HO}(\text{CH}_2\text{CH}_2\text{O})_{400}\text{H}$) and ethylene glycol. The mixture was stirred for 2 h. After that, the solution was added to an autoclave, sealed, kept at $180\text{ }^\circ\text{C}$ for 24 h, cooled, washed and dried at $110\text{ }^\circ\text{C}$ for one night. To make a comparison, pure ethylene glycol was also used to prepare $\text{H}_6\text{V}_4\text{O}_{10}$ in the same procedure.

SEM was performed with a Hitachi S-4800 field emission scanning electron microscope. X-ray diffraction (XRD) was recorded with a PANalytical and X'Pert diffractometer. A Land CT2001A battery tester was used to test the cycling performance of the battery. X-ray photoelectron spectroscopy (XPS) measurements were obtained with an ESCALAB 250 spectrometer. Cyclic voltammetry (CV) was obtained with a Chi660E electrochemical workstation.

$\text{H}_6\text{V}_4\text{O}_{10}$ was found to be an anode and cathode material for lithium and zinc-ion batteries. We pasted the active material, a conductive material (super-pure carbon) and binder polyvinylidene difluoride (PVDF) to a Cu or Al foil in a weight ratio of 7/2/1 as a negative electrode. Li foil was used as a counter electrode. The electrolyte was 1 M LiPF_6 in a 1/1/1 (volume ratio) mixture of ethylene carbonate (EC), propylene carbonate (PC) and dimethyl carbonate (DMC). We also applied $\text{H}_6\text{V}_4\text{O}_{10}$ to aqueous zinc-ion batteries. The active material, a conductive material (super-pure carbon) and binder polyvinylidene difluoride (PVDF) were pasted to a carbon cloth in a weight ratio of 7/2/1. A Zn foil was the counter electrode and the electrolyte was a 1 M ZnSO_4 aqueous solution.

3. RESULTS AND DISCUSSION

SEM images show that the sample prepared with a mixed solvent of polyethylene glycol 400 and ethylene glycol has a mixed morphology of microspheres and nanoparticles in Fig. 1a. The magnified SEM image shows that the surface of the microsphere is modified by loosely distributed nanoparticles

with a size of approximately 100 nm in Fig. 1b. However, the sample prepared with ethylene glycol has uniform microspheres between 3 and 8 μm in diameter, as shown in Fig. 1c. The magnified SEM images show that the surface is composed of tightly packed micro-blocks in Fig. 1d. One possible reason is that ethylene glycol has a lower viscosity than the mixed solvent of polyethylene glycol 400 and ethylene glycol, resulting in different concentration gradients of vanadium precursors. Thus, microspheres with different surface morphologies can be achieved via selecting suitable solvents.

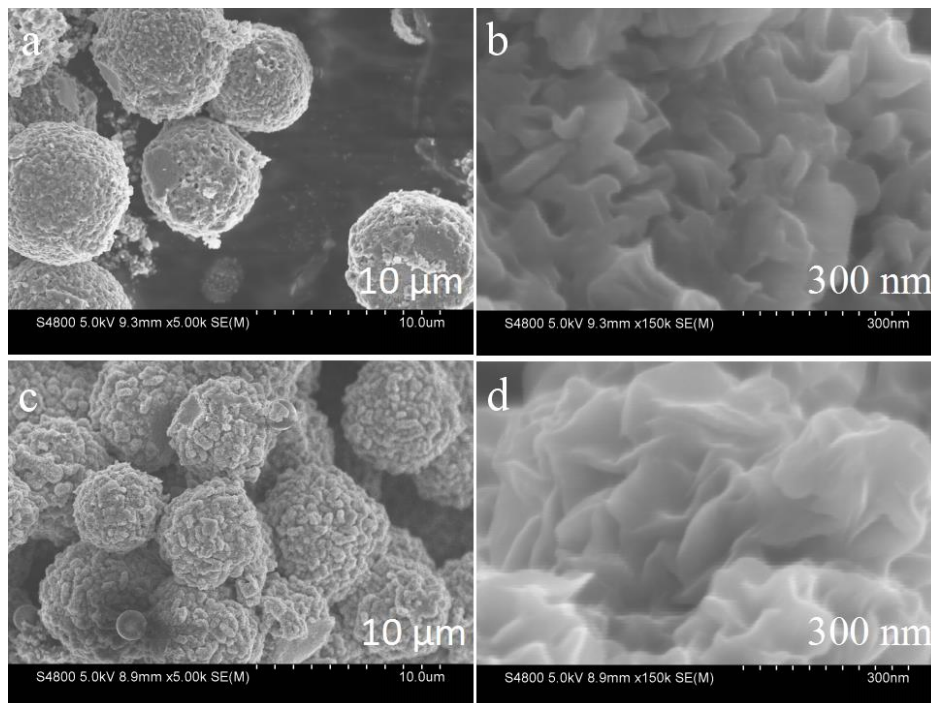


Figure 1. SEM images of samples prepared with the mixed solvent of PEG 400 and ethylene glycol (a), ethylene glycol (c) and their corresponding magnified SEM images of the microsphere surface (b, d), respectively.

X-ray diffraction (XRD) patterns confirm that the crystalline structure of the microspheres prepared with ethylene glycol was identical to $\text{H}_6\text{V}_4\text{O}_{10}$ (JCPDS 41-095), as shown in Fig. 2a. Preparing the other sample with the mixed solvent shows wider and higher intensity peaks, which are also ascribed to $\text{H}_6\text{V}_4\text{O}_{10}$ (JCPDS 41-095), as shown in Fig. 2b. However, impurities were also found due to the appearance of small peaks at 41.35° and 47.14° . One possible reason is that NH_4VO_3 reacts with ethylene glycol to form a vanadyl glycolate precursor. Different concentrations of vanadyl glycolate and denser PEG 400 would result in the formation of byproducts.

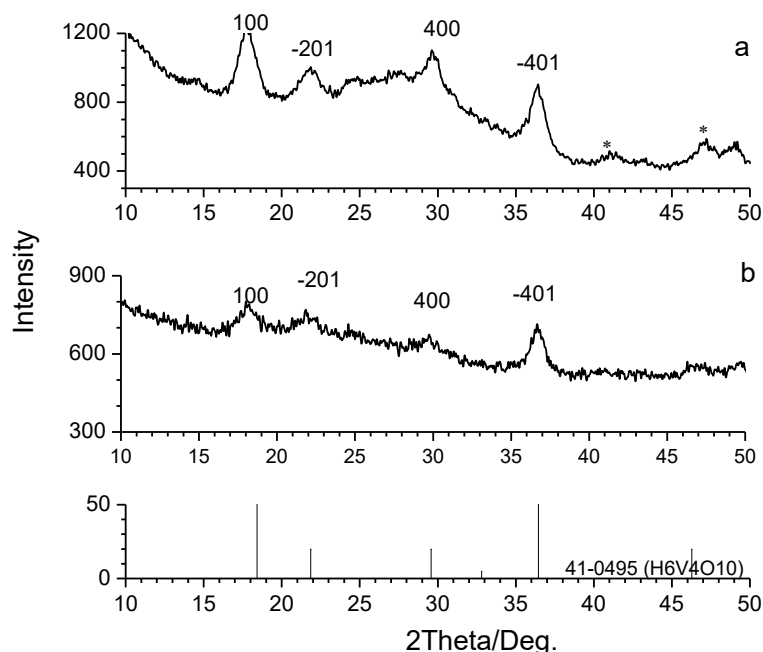


Figure 2. Wide-angle powder XRD patterns of samples prepared with ethylene glycol (a) and the mixed solvent of PEG 400 and ethylene glycol (b).

X-ray photoelectron spectroscopy (XPS) was further performed to investigate the surface of $H_6V_4O_{10}$ microspheres prepared with a mixed solvent of polyethylene glycol 400 and ethylene glycol. The XPS spectra of the O 1s region for $H_6V_4O_{10}$ microspheres show two peaks at 530.2 and 531.2 eV, as shown in Fig. 3, corresponding to O^{2-} and C=O [14], respectively. The V 2p_{3/2} peak is at 517.3 and 516.4 eV, which are ascribed to V (V) and V (IV), respectively [15]. The results show that there is no V (III) on the surface of the samples prepared with polyethylene glycol 400 and ethylene glycol.

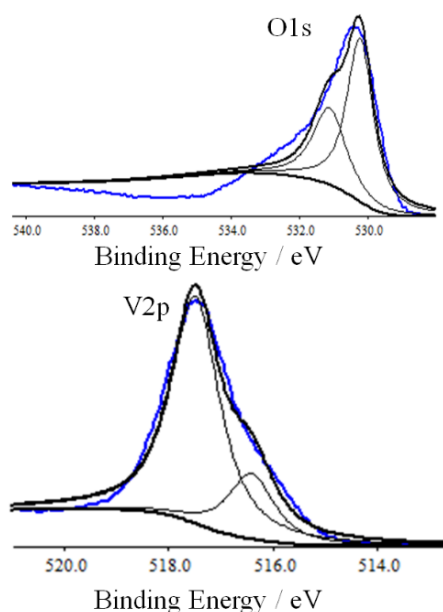


Figure 3. O1s and V2p XPS spectra of the sample prepared with the mixed solvent of PEG 400 and ethylene glycol.

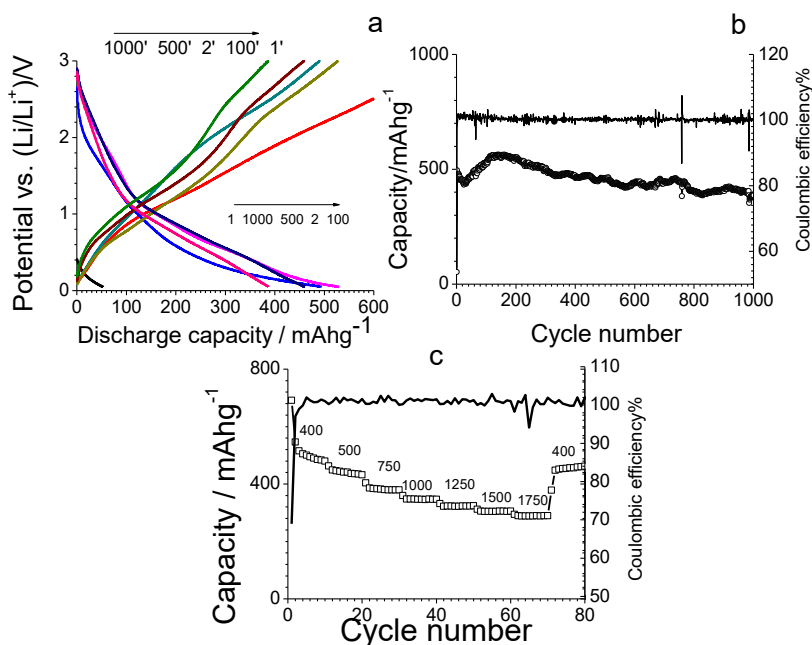


Figure 4. The 1st, 2nd, 100th, 500th and 1000th charge-discharge profiles of H₆V₄O₁₀ microspheres prepared with the mixed solvent of PEG 400 and ethylene glycol/Li cells (a); the cyclic performance at a current density of 400 mA g⁻¹ (b); and the corresponding evolution of reversible capacity at current densities of 400, 500, 750, 1000, 1250, 1500, 1750 and 400 mA g⁻¹ using 0.05–3.0 V potential window (c).

There are few reports on the electrochemical properties of H₆V₄O₁₀ in the literature. We first tested it as an electrode material for lithium and zinc-ion batteries. Fig. 4 shows the anode performance of H₆V₄O₁₀ microspheres prepared with the mixed solvent of polyethylene glycol 400 and ethylene glycol. Fig. 4a shows the 1st, 2nd, 100th, 500th and 1000th charge-discharge profiles at a current density of 400 mA g⁻¹. The electrode has discharge capacities up to 52, 494, 530, 459 and 387 mAh g⁻¹ for the 1st, 2nd, 100th, 500th and 1000th cycles, respectively. A low open circuit voltage of 0.42 V results in a low initial discharge capacity. The discharge capacity retention is up to 78.3% after 1000 cycles corresponding to the second cycle. The coulombic efficiency is approximately 100%, as shown in Fig. 4b. Fig. 4b shows that the H₆V₄O₁₀ electrode materials can steadily cycle at a current density of 400 mA g⁻¹ for 1000 cycles. The H₆V₄O₁₀ electrode materials also exhibit good rate performance at current densities of 400, 500, 750, 1000, 1250, 1500, 1750 and 400 mA g⁻¹ for 80 cycles (Fig. 4c). The capacity retention is 84.4% after 80 cycles with a coulombic efficiency near 100% in Fig. 4c. Notably, a solvo-thermal route is often used to prepare various V₂O₅ microsphere cathode materials for lithium-ion batteries[16-23]. Few reports on vanadium-based microspheres have been found to be anode materials for lithium-ion batteries.

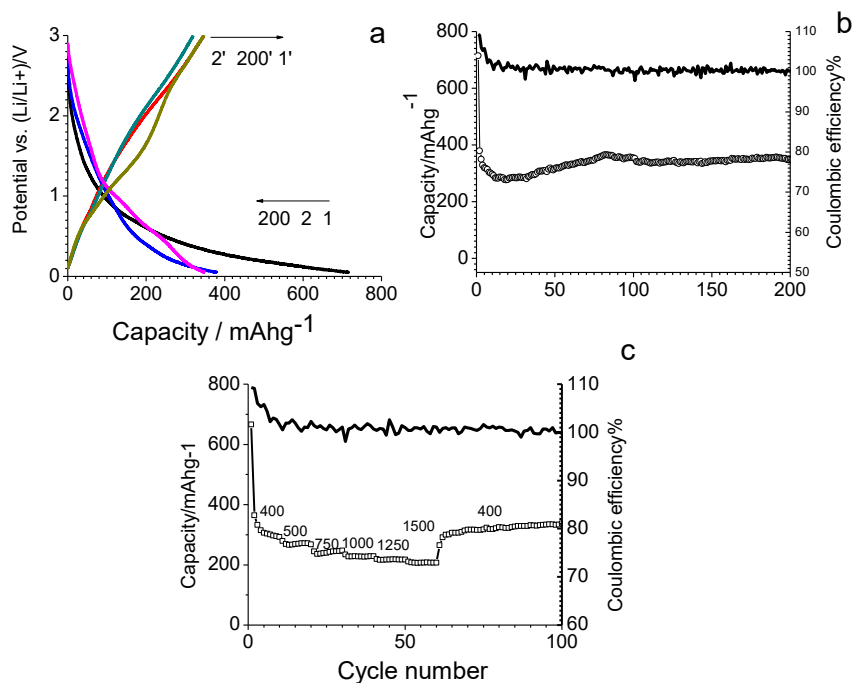


Figure 5. The 1st, 2nd and 200th charge-discharge profiles of H₆V₄O₁₀ microspheres prepared with ethylene glycol/Li cells (a); the cyclic performance at a current density of 400 mA g⁻¹ (b); and the corresponding evolution of the reversible capacity at current densities of 400, 500, 750, 1000, 1250, 1500 and 400 mA g⁻¹ using a 0.05-3.0 V potential window (c).

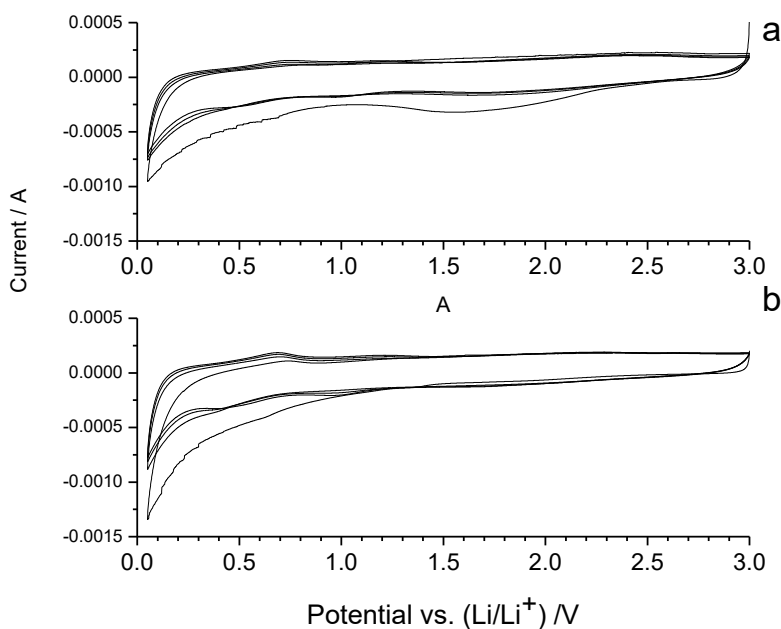


Figure 6. Cyclic voltammograms of H₆V₄O₁₀ microspheres for lithium-ion batteries prepared with ethylene glycol (a).

Fig. 5 shows the anode performance of H₆V₄O₁₀ microspheres prepared with ethylene glycol. Fig. 5a shows the 1st, 2nd and 200th charge-discharge profiles at a current density of 400 mA g⁻¹. The discharge capacities of the electrode are 714, 379 and 348 mA h g⁻¹ for the 1st, 2nd and 200th cycles,

respectively. The capacity retention is 91.8% after 200 cycles compared with the second cycle. Fig. 5b shows that $\text{H}_6\text{V}_4\text{O}_{10}$ microspheres prepared with ethylene glycol electrode materials could steadily cycle at current densities of 400 mA h g^{-1} for 200 cycles. The coulombic efficiency is near 100%, as shown in Fig. 5b. It is even stable in multiple insertion/extraction processes at current densities of 400, 500, 750, 1000, 1250, 1500 and 400 mA g^{-1} for 100 cycles (Fig. 5c). The capacity retention is up to 100% after 100 cycles. The coulombic efficiency is approximately 100% in Fig. 5c. Sealing the cells quickly along with improving the assembly of batteries and nanostructured electrode materials would make a great contribution to reducing the large coulombic efficiency loss in the first cycle. The $\text{H}_6\text{V}_4\text{O}_{10}$ microspheres prepared with the mixed solvent of polyethylene glycol 400 and ethylene glycol show higher discharge capacity than those prepared with ethylene glycol. The mixed solvent microspheres can be stably cycled at larger current densities than the $\text{H}_6\text{V}_4\text{O}_{10}$ microspheres prepared with ethylene glycol.

Cyclic voltammetry (CV) was further performed to study the lithium intercalation for $\text{H}_6\text{V}_4\text{O}_{10}$ microspheres. The first CV curve of $\text{H}_6\text{V}_4\text{O}_{10}$ microspheres prepared with ethylene glycol presents one cathodic peak at 1.57 V, as shown in Fig. 6a, which disappears after the following three cycles. Two small peaks centred at 0.5 and 1.0 V appear in the second, third and fourth cycles. For the CV curves of $\text{H}_6\text{V}_4\text{O}_{10}$ microspheres prepared with ethylene glycol and polyethylene glycol 400 in Fig. 6b, there are no cathodic peaks in the first cycle. A small peak at 0.98 V appears from the second to the fourth cycles. However, a smaller peak at 0.43 V was found in the third and fourth cycles. It can be seen that lithium ions can be reversibly intercalated and deintercalated at approximately 0.43 and 1.0 V for $\text{H}_6\text{V}_4\text{O}_{10}$ microspheres prepared with ethylene glycol and polyethylene glycol 400. This is why it shows a higher discharge capacity and good rate cycling performance. The improved electrochemical performance can be ascribed to nanoparticles modifying the loose surface, which promotes ion and electron transfer.

We also tested the two microspheres as anode materials for aqueous zinc-ion batteries. $\text{H}_6\text{V}_4\text{O}_{10}$ microspheres prepared with ethylene glycol and polyethylene glycol 400 also show higher discharge capacity and better cycling stability. CV curves show that microspheres prepared with ethylene glycol (Sam sp-1) cannot be intercalated-deintercalated due to the absence of peaks in all four cycles, as shown in Fig. 7b. The microspheres prepared with the mixed solvent (Sam sp-1) show a pair of peaks at approximately 0.5 and 0.68 V in Fig. 7a. The second discharge capacity of Sample sp-1 is as high as $238.8 \text{ mA h g}^{-1}$. It has stable cycling of up to 26 cycles with a final discharge capacity of $209.7 \text{ mA h g}^{-1}$, as shown in Fig. 8a'. The capacity retention rate is calculated to be 87.8%. Unfortunately, the coulombic efficiency is not stable due to the appearance of disorder scatter dots, as shown in Fig. 8. Sam sp-2 has a second discharge capacity of $118.7 \text{ mA h g}^{-1}$ in Fig. 8b'. The capacity decays to 43.7 mA h g^{-1} after 14 cycles. The corresponding evolution of reversible capacities with coulombic efficiency for microspheres from PEG 400 and ethylene glycol and microspheres from ethylene glycol at current densities of 50, 100, 200, 300, 400, 500, 750 and 50 mA g^{-1} are shown in Fig. 8b, c, respectively. The $\text{H}_6\text{V}_4\text{O}_{10}$ microspheres (Fig. 8b) prepared with the mixed solvent shows a higher discharge capacity than that prepared with ethylene glycol (Fig. 8c). The cycling stability of the $\text{H}_6\text{V}_4\text{O}_{10}$ microspheres is worse than the reported references on vanadium-based materials for different battery assembly technologies and carbon cloths [24-45].

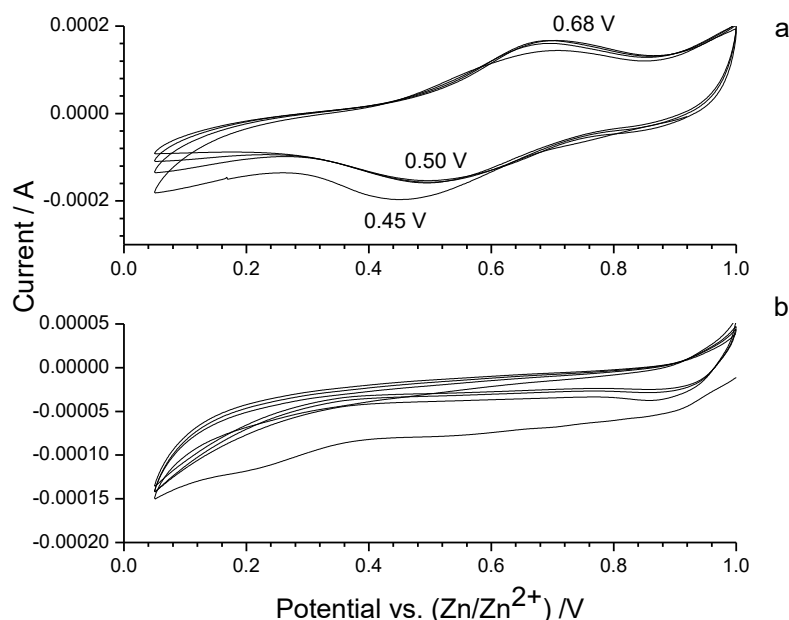


Figure 7. Cyclic voltammograms of $H_6V_4O_{10}$ microspheres for zinc-ion batteries prepared with the mixed solvent of PEG 400 and ethylene glycol (a) and ethylene glycol (b).

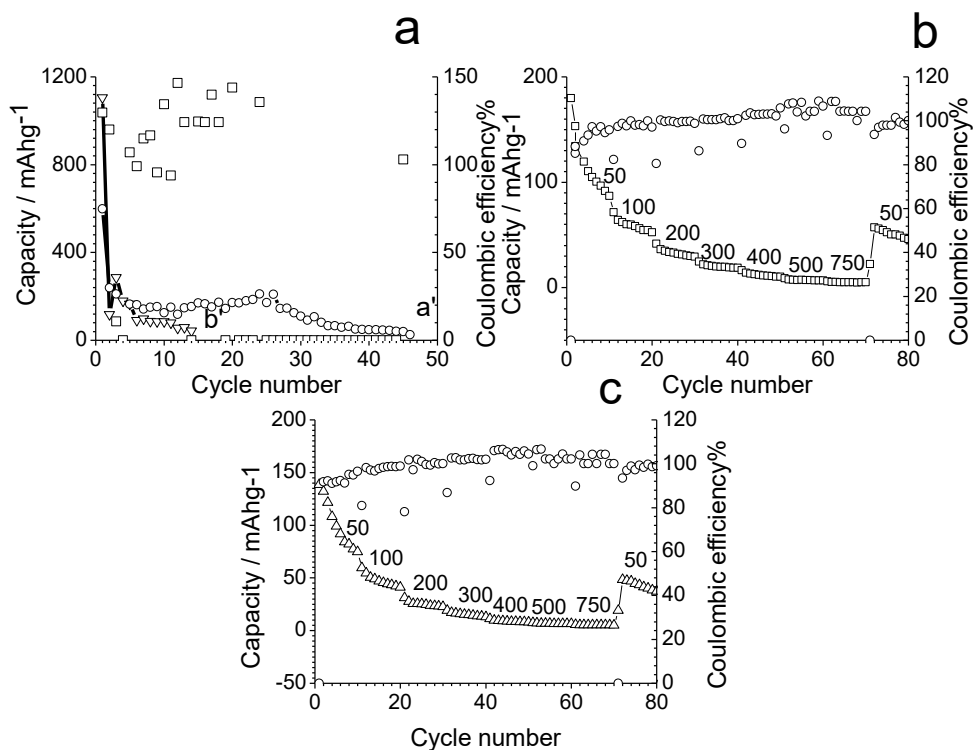


Figure 8. The cyclic performance of $H_6V_4O_{10}$ at a current density of 50 mA g^{-1} for aqueous zinc-ion batteries (a) prepared with the mixed solvent of PEG 400 and ethylene glycol (a') and ethylene glycol (b'); the corresponding evolution of reversible capacities with coulombic efficiency at current densities of 50, 100, 200, 300, 400, 500, 750 and 50 mA g^{-1} using 0.05-1.1 V potential windows for the PEG 400 and ethylene glycol (b) and ethylene glycol (c), respectively.

The $\text{H}_6\text{V}_4\text{O}_{10}$ microspheres may be characteristic of intercalation reactions. If the discharge products are $\text{Li}_x\text{H}_6\text{V}_4\text{O}_{10}$ and $\text{Zn}_y\text{H}_6\text{V}_4\text{O}_{10}$, the calculated x and y are 6.81 and 3.29 based on the second discharge capacity at a current density of 50 mA g^{-1} , respectively. A possible mechanism of the Li/Zn-ion storage mechanism is as follows: $6.81\text{Li}^+ + \text{H}_6\text{V}_4\text{O}_{10} \leftrightarrow \text{Li}_{6.8}\text{H}_6\text{V}_4\text{O}_{10}$; $3.29\text{Zn}^{2+} + \text{H}_6\text{V}_4\text{O}_{10} \leftrightarrow \text{Zn}_{3.29}\text{H}_6\text{V}_4\text{O}_{10}$.

4. CONCLUSIONS

In this study, a straightforward procedure was performed for the preparation of $\text{H}_6\text{V}_4\text{O}_{10}$ microspheres for the first time. $\text{H}_6\text{V}_4\text{O}_{10}$ microspheres modified by loosely distributed nanoparticles were achieved by selecting a mixed solvent of ethylene glycol and polyethylene glycol 400. Mono-dispersed microspheres tightly packed with micro-blocks were prepared with ethylene glycol for higher viscosity. The former showed higher discharge capacity and better rate cycling performance than that of the latter for lithium and zinc-ion batteries, which can be ascribed to the nanoparticles that modify the loose surface and promote ion and electron transfer. Further work will be concentrated on the preparation of hierarchical $\text{H}_6\text{V}_4\text{O}_{10}$ nanostructures with an application to the field of Mg-ion batteries and O_2/H_2 evolution.

ACKNOWLEDGEMENTS

The project was supported by 111 project, B12015.

References

1. N. Zhang, F.Y. Cheng, Y.C. Liu, Q. Zhao, K.X. Lei, C.C. Chen, X.S. Liu, J. Chen, *J. Am. Chem. Soc.*, 138 (2016) 12894-12901.
2. Q.H. Wang, J.T. Xu, W.C. Zhang, M.L. Mao, Z.X. Wei, L. Wang, C.Y. Cui, Y.X. Zhu, J.M. Ma, *J. Mater. Chem. A*, 6 (2017) 8815-8838.
3. M.S. Liu, B. Su, Y. Tang, X.C. Jiang, A.B. Yu, *Adv. Energy Mater.*, 7 (2017) 1700885.
4. G.H. Jeong, I. Lee, D. Lee, H.M. Lee, S. Baek, O.P. Kwon, P.N. Kumta, S. Yoon, S.W. Kim, *Nanotechnology*, 29 (2018) 195403.
5. H.L. Fei, X.M. Wu, H. Li, M.D. Wei, *J. Colloid Interf., Sci.*, 415 (2014) 85-88.
6. H.L. Fei, Z.R. Shen, J.G. Wang, H.J. Zhou, D.T. Ding, T.H. Chen, *J. Power Sources*, 189 (2009) 1164-1166.
7. H.L. Fei, Z.R. Shen, J.G. Wang, H.J. Zhou, D.T. Ding, T.H. Chen, *Electrochem. Commun.*, 10 (2008) 1541-1544.
8. H.L. Fei, H. Li, Z.W. Li, W.J. Feng, X. Liu, M.D. Wei, *Dalton T.*, 43 (2014) 16522-16527.
9. X.M. Shi, J.C. Li, X.Y. Lang, Q. Jiang, *J. Phys. Chem. C*, 121 (2017) 5974-5982.
10. V.C. Srivastava, S. Gupta, K.N. Rai, J. Kumar, *Mater. Res. Bull.*, 23 (1988) 341-348.
11. X.S. Zhou, L. Yu, X.W. Lou, *Nanoscale*, 8 (2016) 8384-8389.
12. W.S. Weng, J. Lin, Y.C. Du, X.F. Ge, X.X. Zhou, J.C. Bao, *J. Mater. Chem. A*, 6 (2018) 10168-10175.
13. I. Mjejri, F. Sediri, *Ionics*, 2019, doi.org/10.1007/s11581-019-02929-2.

14. G. Silversmit, D. Depla, H. Poelman, G.B. Marin, R. De Gryse, *J. Electron Spectrosc. Relat. Phenom.*, 135 (2004) 167-175.
15. J. Mendiàdua, R. Casanova and Y. Barbaux, *J. Electron Spectrosc. Relat. Phenom.*, 71 (1995) 249-261.
16. K. Kim, M.J. Lee, *Electrochim. Acta*, 258 (2017) 942-950.
17. Y.J. Dong, H.Y. Wei, W. Liu, Q.J. Liu, W.J. Zhang, Y.Z. Yang, *J. Power Sources*, 285 (2015) 538-542.
18. B. Yan, X.F. Li, Z.M. Bai, Y. Zhao, L. Dong, X.S. Song, D.J. Li, G. Langford, X.L. Sun, *Nano Energy*, 24 (2016) 32-44.
19. P.Y. Chen, G.T. Zheng, G.Z. Guo, Z.C. Wang, J. Tang, S. Li, Z.S. Wen, S.J. Ji, J.C. Sun, *J. Alloys Compd*, 784 (2019) 574-583.
20. Y.L. Shan, L. Xu, Y.J. Hu, H. Jiang, C.Z. Li, *Chem. Eng. Sci.*, 200 (2019) 38-45.
21. X.X. An, Q. Su, Y.L. Liu, A.Q. Pan, *Int. J. Electrochem. Sci.*, 12 (2017) 6885-6894.
22. E. Uchaker, N. Zhou, Y.W. Li, G.Z. Cao, *J. Phys. Chem. C* 117 (2013) 1621-1626.
23. H.E. Wang, D.S. Chen, Y. Cai, R.L. Zhang, J.M. Xu, Z. Deng, X.F. Zheng, Y. Li, I. Bello, B.L. Su, *J. Colloid Interf. Sci.*, 418 (2014) 74-80.
24. H.G. Qin, Z. Yang, L.L. Xi Chen, L.M. Wang, *J. Mater. Chem. A*, 6 (2018) 23757-23765.
25. C. Kim, B.Y. Ahn, T.S. Wei, Y.J. Jo, S. Jeong, Y.M. Choi, I.D. Kim, J.A. Lewis, *ACS Nano*, 12 (2018) 11838-11846.
26. L.L. Wang, X. Cao, L.H. Xu, J.T. Chen, J.R. Zheng, *ACS Sustain. Chem. Eng.*, 6 (2018) 16055-16063.
27. T.Y. Wei, Q. Li, G.Z. Yang, C.X. Wang, *J. Mater. Chem. A*, 6 (2018) 20402-20410.
28. Y.Q. Yang, Y. Tang, G.Z. Fang, L.T. Shan, J.S. Guo, W.Y. Zhang, C. Wang, L.B. Wang, J. Zhou, S.Q. Liang, *Energ. Environ. Sci.*, 11 (2018) 3157-3162.
29. T.Y. Wei, Q. Li, G.Z. Yang, C.X. Wang, *Electrochim. Acta*, 287 (2018) 60-67.
30. J. Xin, C. Liu, Z.W. Qiu, J.J. Zhou, Q. Wang, Y. Li, B.K. Guo, *RSC Adv.*, 8 (2018) 26906-26909.
31. F. Wan, L.L. Zhang, X. Dai, X.Y. Wang, Z.Q. Niu, J. Chen, *Nat. Commun.*, 9 (2018) 1656.
32. B.Z. Jiang, C.J. Xu, C.L. Wu, L.B. Dong, J. Li, F.Y. Kang, *Electrochim. Acta*, 229 (2017) 422-428.
33. M. H. Alfaruqi, V. Mathew, J.J. Song, S. Kim, S. Islam, D.T. Pham, J. Jo, S. Kim, J.P. Baboo, Z.L. Xiu, K.S. Lee, Y.K. Sun, J. Kim, *Chem. Mater.*, 29 (2017) 1684-1694.
34. C. Shen, X. Li, N. Li, K.Y. Xie, J.G. Wang, X.R. Liu, B.Q. Wei, *ACS Appl. Mater. Inter.*, 10 (2018) 25446-25453.
35. N. Zhang, M. Jia, Y. Dong, Y.Y. Wang, J.Z. Xu, Y.C. Liu, L.F. Jiao, F.Y. Cheng, *Adv. Func. Mater.*, 29 (2019) 1807331
36. L.N. Chen, Y.S. Ruan, G.B. Zhang, Q.L. Wei, Y.L. Jiang, T.F. Xiong, P. He, W. Yang, M.Y. Yan, Q.Y. An, L.Q. Mai, *Chem. Mater.*, 31 (2019) 699-706.
37. N. Zhang, Y. Dong, M. Jia, X. Bian, Y.Y. Wang, M.D. Qiu, J.Z. Xu, Y.C. Liu, L.F. Jiao, F.Y. Cheng, *ACS Energy Lett.*, 3 (2018) 1366-1372.
38. D. Kundu, B.D. Adams, V. Duffort, S. Hosseini Vajargah and L.F. Nazar, *Nat. Energy*, 1 (2016) 16119.
39. Q. Pang, C.L. Sun, Y.H. Yu, K.N. Zhao, Z.Y. Zhang, P.M. Voyles, *Adv. Energy Mater.*, 19 (2018) 1800144.
40. C. Chen, M. Zhou, C. Chen, Q.Y. An, P. Luo, *J. Alloy Compd.*, 787 (2019) 9-16.
41. D. Bin, Y. Liu, B.B. Yang, J.H. Huang, X.L. Dong, X. Zhang, Y.G. Wang, Y.Y. Xia, *ACS Appl. Mater. Inter.*, 2019, DOI:10.1021/acsami.9b03159.
42. F. Wan, Z.Q. Niu, *Angew Chem. Int. Edit.*, 2019, DOI:10.1002/anie.201903941.
43. M. Ulaganathan, S. Suresh, P. Periasamy and R. Pitchai, *ACS Sustain. Chem. Eng.*, 7 (2019) 6053-6060.
44. N. Zhang, M. Jia, Y. Dong, Y.Y. Wang, J.Z. Xu, Y.C. Liu, L.F. Jiao, F.Y. Cheng, *Adv. Func. Mater.*, 29 (2019) 1807331.

45. Z.Q. Xie, J.W. Lai, X.P. Zhu, Y. Wang, *ACS Applied. Energy Mater.*, 1 (2018) 6401-6408

© 2019 The Authors. Published by ESG (www.electrochemsci.org). This article is an open access article distributed under the terms and conditions of the Creative Commons Attribution license (<http://creativecommons.org/licenses/by/4.0/>).